

Revisit the periodicity of SGR J1935+2154 bursts with updated sample

Sheng-Lun Xie^{1,2}, Ce Cai^{2,9}, Shao-Lin Xiong^{2*}, Yun-Wei Yu^{1†}, Yan-Qiu Zhang^{2,3}, Lin Lin⁴, Zhen Zhang², Wang-Chen Xue^{2,3}, Jia-Cong Liu^{2,3}, Yi Zhao^{2,4}, Shuo Xiao^{2,3}, Chao Zheng^{2,3}, Qi-Bin Yi^{2,5}, Peng Zhang², Ping Wang², Rui Qiao², Wen-Xi Peng², Yue Huang², Xiang Ma², Xiao-Yun Zhao², Xiao-Bo Li², Shi-Jie Zheng², Ming-Yu Ge², Cheng-Kui Li², Xin-Qiao Li², Xiang-Yang Wen², Fan Zhang², Li-Ming Song², Shuang-Nan Zhang², Zhi-Wei Guo^{2,6}, Xiao-Lu Zhang^{2,7}, Guo-Ying Zhao^{2,5}, Chao-Yang Li^{2,8}

¹ *Institute of Astrophysics, Central China Normal University, Wuhan 430079, China*

² *Key Laboratory of Particle Astrophysics, Institute of High Energy Physics, Chinese Academy of Sciences, 19B Yuquan Road, Beijing 100049, China*

³ *University of Chinese Academy of Sciences, Chinese Academy of Sciences, Beijing 100049, China*

⁴ *Department of Astronomy, Beijing Normal University, Beijing 100088, People's Republic of China*

⁵ *Department of Physics, Xiangtan University, Xiangtan, Hunan Province 411105, China*

⁶ *College of physics Sciences Technology, Hebei University, No. 180 Wusi Dong Road, Lian Chi District, Baoding City, Hebei Province 071002, China*

⁷ *College of Physics and Engineering, Qufu Normal University, Qufu 273165, China*

⁸ *Physics and Space Science College, China West Normal University, Nanchong 637002, China*

⁹ *College of Physics, Hebei Normal University, 20 South Erhuan Road, Shijiazhuang 050024, Hebei, China*

Accepted XXX. Received YYY; in original form ZZZ

ABSTRACT

Since FRB 200428 has been found to be associated with an X-ray burst from the Galactic magnetar SGR J1935+2154, it is interesting to explore whether the magnetar bursts also follow the similar active periodic behavior as some repeating FRBs. Previous studies show that there is possible period about 230 day in SGR J1935+2154 bursts. Here, we collected an updated burst sample from SGR J1935+2154, including all bursts reported by Fermi/GBM and GECAM till 2022 January. We also developed a targeted search pipeline to reveal more bursts from SGR J1935+2154 in the Fermi/GBM data from 2008 August to 2014 December (i.e. before the first burst detected by Swift/BAT). With this burst sample, we re-analyzed the possible periodicity of SGR J1935+2154 bursts using the Period Folding and Lomb–Scargle Periodogram methods. Our results show that the periodicity ~238 day reported in literature is probably fake and the observation effects may introduce false periods (i.e. 55 day) according to simulation tests. We find that, for the current burst sample, the most probable period is 126.88 ± 2.05 day, which could be interpreted as the precession of the magnetar. However, we note that the whole burst history is very complicated and difficult to be perfectly accommodated with any period reported thus far, therefore more monitoring observations of SGR J1935+2154 are required to test any periodicity hypothesis.

Key words: methods: data analysis - stars: magnetars

1 INTRODUCTION

Highly-magnetized neutron stars called magnetars are perceived as the nature of soft gamma-ray repeaters (SGRs) and anomalous X-ray pulsars (AXPs), which can intermittently produce gamma/X-ray bursts (Duncan & Thompson 1992; van Kerkwijk et al. 1995; Kouveliotou et al. 1998; Banas et al. 1997; Kaspi & Beloborodov 2017). On April 28th, 2020, it was discovered that a fast radio burst (FRB 200428, Li et al. 2021b; Bochenek et al. 2020; CHIME/FRB Collaboration et al. 2020b) was produced by the Galactic magnetar SGR J1935+2154 and this FRB was in temporal coincidence with an non-thermal X-ray burst from the magnetar (Li et al. 2021b; Mereghetti et al. 2020; Tavani et al. 2020; Ridnaia et al. 2021).

FRBs are super bright radio pulses with a duration of a few milliseconds (Lorimer et al. 2007; Thornton et al. 2013), featuring in their abnormally high dispersion measures (DMs). Since the first discovery of the Lorimer burst from the pulsar data of Parkes radio telescope (Lorimer et al. 2007), over 600 FRBs have been found (Petroff et al. 2016), which enabled us to learn more characteristics of the FRBs, such as the localization of their host galaxies (Chatterjee et al. 2017; Bannister et al. 2019; Ravi et al. 2019; Macquart et al. 2020; Marcote et al. 2020), polarization, rotation measure and the highly magnetic environment around the sources (Michilli et al. 2018). According to their potential cosmological origin, FRBs have been widely connected to some violent activities and even catastrophic coalescences or collapses of compact binaries or objects (see Platts et al. (2019)¹ for a review).

* E-mail: xiongs1@ihep.ac.cn (SLX)

† E-mail: yuyw@ccnu.edu.cn (YWY)

¹ <https://frbtheorycat.org>

Table 1. Spectral models used in the targeted search for X-ray bursts from SGR J1935+2154.

Spectrum Template	alpha	beta	Epeak or kT (keV)
Band	0.06	-5.3	35
BlackBody	9
Comptonized	0.5	...	35
OTTB	32
Powerlaw	-2	...	100

Although most FRBs were observed to be one-off burst, several repeating sources have been discovered, such as FRB 121102, FRB 180916, FRB 20190520B, FRB 20181030A, and FRB 20201124A (Spitler et al. 2016; Chatterjee et al. 2017; Marcote et al. 2017; Tendulkar et al. 2017). Undoubtedly, the repetition of these FRBs disfavors the models involving catastrophic events and, instead, strongly supports the activities of compact objects, in particular, young magnetars (Popov & Postnov 2010; Kulkarni et al. 2014; Connor et al. 2016; Cordes & Wasserman 2016; Katz 2016; Lyutikov 2017; Metzger et al. 2017; Cao et al. 2017). This hypothesis has further been confirmed by the discovery of the association of FRB 200428 with an X-ray burst from SGR J1935+2154 (Li et al. 2021b; Mereghetti et al. 2020; Tavani et al. 2020; Ridnaia et al. 2021). This discovery not only provides an important constraint on the physical mechanisms responsible for the FRB phenomena (e.g., Lu et al. 2020; Margalit et al. 2020; Wu et al. 2020; Yang et al. 2020; Zhang 2020b; Yu et al. 2021), but also hints that we may use the X-ray bursts of magnetars to indirectly probe the temporal behavior of the repeating FRBs.

It is worthy to note that repeating FRBs could have periodic window behavior (PWB), e.g. FRB 180916 was found to have a possible period of 16.35 ± 0.15 days (CHIME/FRB Collaboration et al. 2020a), and FRB 121102 could be with a period of 156 days (Rajwade et al. 2020; Cruces et al. 2021). Therefore, it is very interesting to investigate whether the activities of SGR J1935+2154, which has emitted FRB 200428, also have a PWB. This has been studied by some previous works: Denissenya et al. (2021) argued a period of 231 days, using likelihood analysis with the data of IPN (Interplanetary Network) instruments from 2014 July to 2021 February; Grossan (2021) estimated a possible period of about 231 days by analyzing the observations from IPN from 2014 July to 2020 May; Zou et al. (2021) suggested that the period is about 238 days using the data of Fermi/GBM (Fermi Gamma-ray Burst Monitor) from 2014 July to 2021 October.

In this paper, we carry out a comprehensive targeted search on X-ray bursts of SGR J1935+2154 using Fermi/GBM (Meegan et al. 2009) data from 2008 August to 2014 December. We also collect the most recent burst samples from Fermi/GBM and all bursts detected by GECAM (Gravitational wave high-energy Electromagnetic Counterpart All-sky Monitor, Li et al. 2021a; Xiao et al. 2022) during its first year of observation. With more bursts covering a longer time interval than previous studies (Denissenya et al. 2021; Grossan 2021; Zou et al. 2021), we hope to make a better constraint on the periodicity searching. In Section 2, we present the search process and report the burst candidates. In Section 3, we use the Period Folding and Lomb-Scargle algorithm to search the possible periodic active window. Finally, the summary and discussion are given in Section 4.

2 TARGETED SEARCH FOR BURSTS

SGR J1935+2154 is a Galactic magnetar, which was first found by the Swift Burst Alert Telescope (BAT) in 2014 (Stamatikos et al. 2014). It has experienced four active episodes before 2020, respectively (Younes et al. 2017; Lin et al. 2020b,c). Since 2021, there exist at least 3 active episodes so far.

Targeted sub-threshold search for bursts from SGR J1935+2154 is very important, because there are potential bursts which are rather weak and unable to trigger the instrument with normal threshold. Many works show evidence that some SGR bursts did not trigger detector (Lin et al. 2020a,b,c; Mereghetti et al. 2020; Younes et al. 2020; Yang et al. 2021; Zou et al. 2021). However, some of previous studies only searched SGR bursts after the first reported burst by Swift/BAT in 2014 and ignored the time interval before 2014. In this paper, we implement a targeted search on Fermi/GBM Continuous high time resolution (CTIME) and Time-tagged events (TTE)² from 2008-08-12 to 2014-12-31 (UTC) with the coherent search method (Blackburn et al. 2015; Cai et al. 2021).

We have developed a pipeline to search for gamma-ray bursts (GRBs) and SGRs using the traditional signal-to-noise ratio (SNR) method for blind search and the coherent search method for targeted search (e.g., Cai et al. 2021). In this targeted search for SGR J1935+2154 bursts, we use 5 spectral templates (see Table 1) and set the trigger threshold of Log-Likelihood Ratio (LR) to be 20. Thousands of burst candidates have been found, and we screened them according to the following criteria:

- (i) Excluding those candidate events when the spacecraft is near the South Atlantic Anomaly (SAA) or the location of SGR J1935+2154 is in the Earth shadow;
- (ii) Excluding those events with the incident angle of most significant detectors greater than 60° and those events which are falsely triggered by the sharp variation of background count rates caused by instrument startup and shutdown. The number of these two kinds of events is about ~ 7400 ;
- (iii) Excluding the solar flares (~ 1800 events), particle events (~ 3800), Terrestrial Gamma Ray Flash (TGF, Briggs et al. 2013) and Terrestrial Electron Beam (TEB, Xiong et al. 2012)^{3,4};
- (iv) Excluding phosphorescence spike events (5 events) (e.g., see Goldstein et al. 2019; Wu et al. 2022), which are listed in Table 2.

Finally, we found 10 new candidate bursts and 3 previously found bursts from SGR J1935+2154 during the time interval from 2008-08-12 to 2014-12-31 (UTC). We call these 10 bursts as candidates because they are solely detected by Fermi/GBM revealed by our targeted search and without confirmation by other instruments, while the other 3 bursts have been found and reported by Swift/BAT (e.g. Lin et al. 2020c). Details of our burst candidates are listed in Table 2. The light curves and location of candidate bursts are shown in Fig. 3 and Fig. 1, respectively. The location is generated by the search pipeline (Cai et al. 2021). Note that the light curve, spectrum and location of these candidate bursts are all consistent with known bursts from SGR J1935+2154, based on which we argue that most of these candidates, if not all, are probably from SGR J1935+2154.

² <https://heasarc.gsfc.nasa.gov/FTP/Fermi/data/gbm/daily/>

³ <https://fermi.gsfc.nasa.gov/ssc/data/access/gbm/tgf/>

⁴ <https://gamma-ray.nsstc.nasa.gov/gbm/science/description.html>

Table 2. The properties of SGR J1935+2154 burst candidates found by our targeted search in this work and the Phosphorescence Spikes Events.

Event Time(UTC)	MaxLR ^a	Significance	Template	Duration (ms)	RA (°)	DEC (°)	Err (°)	BlackBody		
								kT	Flux ^b	C-Stat/dof
2008-11-30T02:13:00	22.16	6.74	BlackBody	<256	285.94	28.3	14.99	3.69 ^{+2.57} _{-1.29}	0.39 ^{+0.08} _{-0.16}	12.23/14
2008-12-24T18:19:07	15.24	5.62	BlackBody	<512	299.12	15.39	17.82	18.93 ^{+9.02} _{-5.77}	0.77 ^{+0.23} _{-0.20}	12.23/14
2009-08-02T02:45:03	18.56	6.17	Powerlaw	<512	293.64	29.23	13.14	7.77 ^{+4.28} _{-3.21}	0.59 ^{+0.16} _{-0.20}	15.38/14
2009-12-15T14:41:52	21.6	6.61	Powerlaw	<512	298.24	22.56	10.82	5.96 ^{+6.74} _{-4.43}	0.34 ^{+0.02} _{-0.23}	22.52/14
2011-02-17T06:13:04	49.18	10.05	Comptonized	<256	278.55	14.38	10.32	8.23 ^{+4.21} _{-3.04}	0.63 ^{+0.11} _{-0.16}	21.53/22
2011-07-08T20:26:09	18.95	5.72	Powerlaw	<256	299.45	11.93	16.84	1.39 ^{+0.40} _{-0.30}	0.70 ^{+0.04} _{-0.70}	9.73/14
2013-01-16T21:12:33	20.73	6.59	OTTB	16	277.58	3.21	19.11	7.23 ^{+4.59} _{-3.30}	1.47 ^{+2.14} _{-0.77}	18.92/30
2013-03-08T00:08:58	46.33	6.64	Powerlaw	576	297.35	25.97	6.37	4.40 ^{+2.48} _{-1.69}	1.04 ^{+1.15} _{-0.28}	23.9/30
2013-03-28T05:45:45	23.17	6.93	Powerlaw	32	309.41	3.67	10.34	4.09 ^{+1.84} _{-2.77}	0.85 ^{+0.28} _{-0.68}	7.83/14
2013-05-04T16:20:31	21.32	6.75	Powerlaw	24	309.46	22.36	15.21	7.54 ^{+7.65} _{-3.66}	1.35 ^{+1.95} _{-0.85}	12.78/30
2014-07-05T09:32:48 ^c	209.13	7.44	OTTB	96	298.8	24.39	9	5.56 ^{+1.72} _{-1.28}	2.30 ^{+2.48} _{-2.01}	37.32/46
2014-07-05T09:37:34 ^c	291.28	21.37	Powerlaw	48	290.96	22.06	8.16	6.26 ^{+2.36} _{-1.79}	2.48 ^{+2.86} _{-2.09}	46.73/46
2014-07-05T09:41:06 ^c	26.65	7.34	OTTB	64	301.87	37.49	13.26	12.32 ^{+4.58} _{-3.74}	2.07 ^{+2.63} _{-1.40}	29.18/46

Phosphorescence Spikes Events										
2009-01-28T15:32:06	60.08	12.22	Powerlaw	<256	302.46	12.22	3.75
2010-02-10T13:34:14	317.86	22.73	Powerlaw	<256	287.39	13.19	2.56
2010-12-16T06:03:10	37622.94	233.82	Powerlaw	<256	304.69	31.11	0.46
2014-05-15T15:32:56	34.38	6.97	BlackBody	3	275.49	26.26	22.71
2014-06-24T23:02:10	47.13	9.88	Powerlaw	7	281.95	5.69	16.97

^a Max Log-Likelihood Ratio (Blackburn et al. 2015; Cai et al. 2021)

^b Values in units of 10^{-7} erg cm^{-2} s^{-1} are calculated by using BlackBody Spectrum within 8-200 keV

^c Real burst which are also detected by Swift/BAT

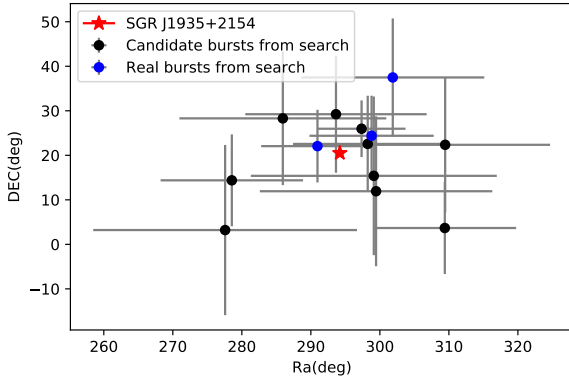


Figure 1. The location of candidate bursts. The red star marks the accurate position of SGR J1935+2154. The black and blue represent the location of candidate bursts and real (confirmed) bursts (i.e. which are also detected by Swift/BAT), respectively. The gray lines mean $1-\sigma$ confidence level.

3 PERIODICITY OF BURST HISTORY

To explore the potential periodicity behavior in the burst history of SGR J1935+2154, we collected all bursts including the recently reported bursts (till 2022 January) from Fermi/GBM and GECAM, as well as the burst candidates we found in Fermi/GBM data from 2008-08-12 to 2014-12-31 (UTC). Fermi/GBM bursts that we used in this study have been reported in literature (Lin et al. 2020b,c; Zou et al. 2021) or in the Gamma-ray Coordinates Network (GCN)⁵. Since Zou et al. (2021) has listed the bursts of Fermi/GBM from 2014 July to 2021 October, we only listed Fermi/GBM bursts from

⁵ <https://gcn.gsfc.nasa.gov/>

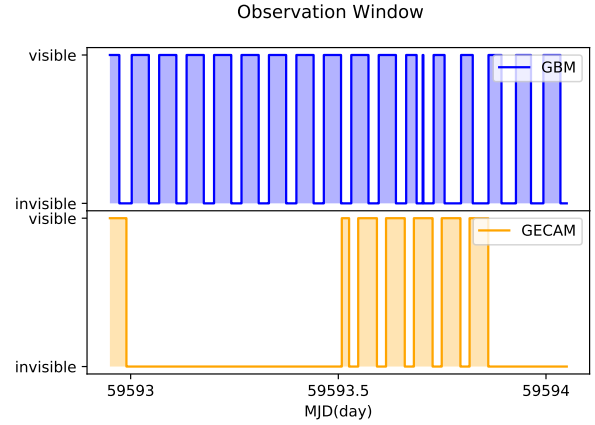


Figure 2. The visible time windows of Fermi/GBM and GECAM to SGR J1935+2154. The exposure time is the union of the Fermi/GBM and GECAM visible time interval in that day.

2021 November to 2022 January in Table 3. The burst sample of GECAM is listed in Table 4.

We divide all bursts into two samples. Sample A contains all reported bursts from Fermi/GBM and GECAM from 2014 July to 2022 January. The start time (T_0) of Sample A is set to 56658 (MJD). This is the main sample for searching the possible periodicity. Sample B is composed of Sample A and candidate bursts found from 2008 to 2014. The start time of Sample B is set to 54771 (MJD). Owing to the small number of the candidate bursts, it has less constraint on the periodicity. Thus sample B is only used to check the periodicity result derived from Sample A.

We note that the setting of the start time (T_0) does not affect the periodicity result, which is confirmed by the simulations (see Section 3.3). We also calculate the visible time windows and the exposure

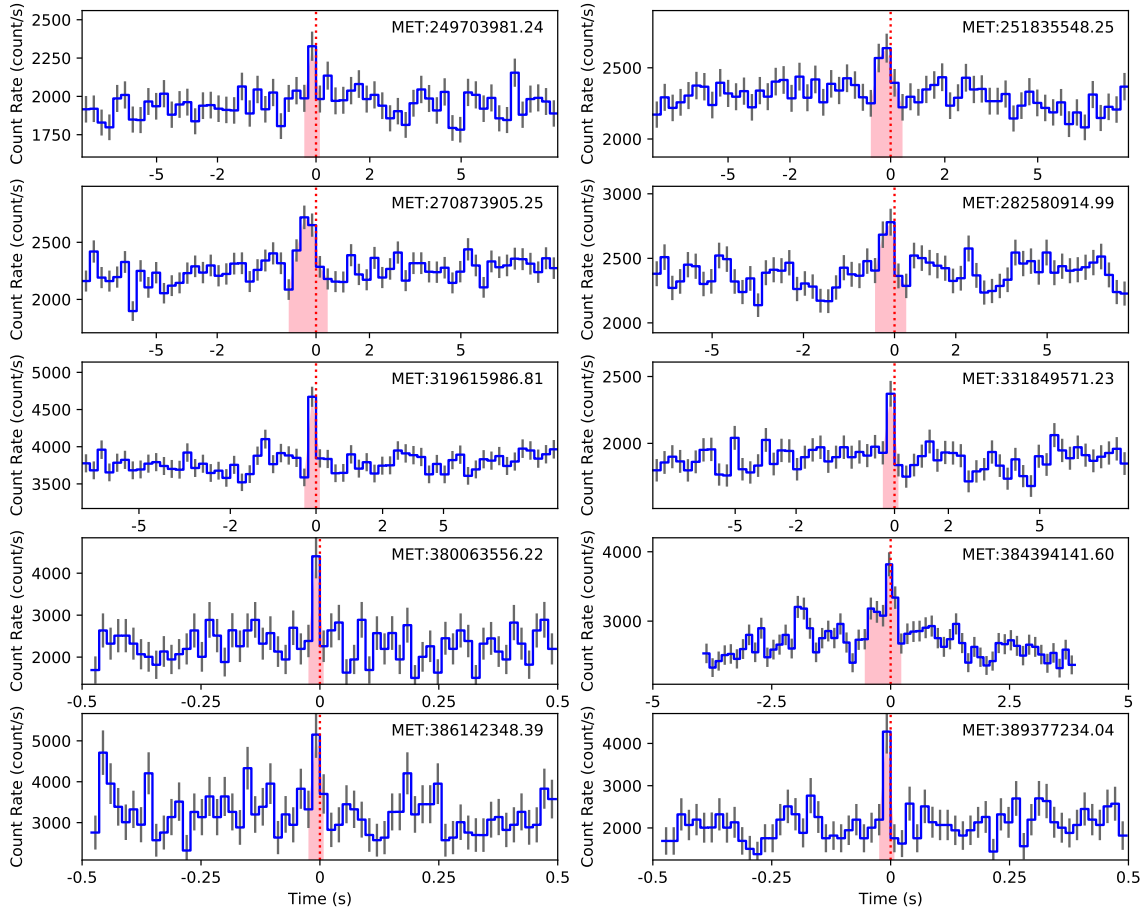


Figure 3. The light curve of candidate bursts from SGR J1935+2154. The blue curves represent the summed light curves of those NaI detectors with significant excess. The red dotted line represent the trigger time and pink shadow is the duration of candidate burst.

time history of SGR J1935+2154 for Fermi/GBM and GECAM respectively, which are used in the periodicity search. An example of the visible time window is shown in Fig 2.

3.1 Period Folding

First, we adopt the Period Folding method to search the possible periodicity, which was used in the FRB studies (CHIME/FRB Collaboration et al. 2020a). We fold the burst times of SGR J1935+2154 with different trial periods and group these folded bursts into n bins, namely the number of phase bins. In this study, we set n for period folding with both samples A & B. In addition, we also use the C -stat test together with Pearson's χ^2 -stat test to examine the significance of the period (with the folded burst numbers in phase bins). The C -stat can be written as

$$C = 2 \sum_{i=1}^n E_i - N_i + N_i \ln(N_i/E_i) \quad (1)$$

where N_i is the number of bursts in the phase bin i , $E_i = pT_i$ is the expected number of bursts in bin i if there is no period, T_i is the exposure time of bin i and $p = \sum N_i / \sum T_i$ is the average burst

rate. Like Reduced χ^2 , we use $(C - C_e)/\sqrt{C_v}$ to assess deviation and significance, where C_e is the expected value and C_v is variance (see Kaastra 2017). The peak of $(C - C_e)/\sqrt{C_v}$ indicate a possible period of bursts.

We set n to 20 and search trial period from $P_{\min} = 0.5$ days to $P_{\max} = 600$ days ($f_{\min} = 1/P_{\max}$, $f_{\max} = 1/P_{\min}$) with step $\Delta f = 0.1/T_{\text{span}}$, where T_{span} mean the longest time from the first burst to the last one. Setting $P_{\max} = 600$ to make sure that there are at least 5 periods in the extent of the whole observation of all bursts. The reduced χ^2 and $(C - C_e)/\sqrt{C_v}$ of two samples (Sample A and Sample B) are shown in the left two panels of Fig 4 and 5, respectively. According to the results of sample A, the peak of reduced χ^2 is 127.31 day, which is the same as the peak of $(C - C_e)/\sqrt{C_v}$. The results of Period Folding are very consistent with that of periodogram method, which is 126.88 day, namely the vertical red dotted line in Fig 4.

We note that, there is a peak around 55 days with similar significance. It should be caused by observation windows, according to the Lomb-Scargle Periodogram of simulation data of observation windows (see Section 3.2). The peaks of χ^2 and $(C - C_e)/\sqrt{C_v}$ of sample B are 127.86 day, respectively, which is well consistent with the result of sample A.

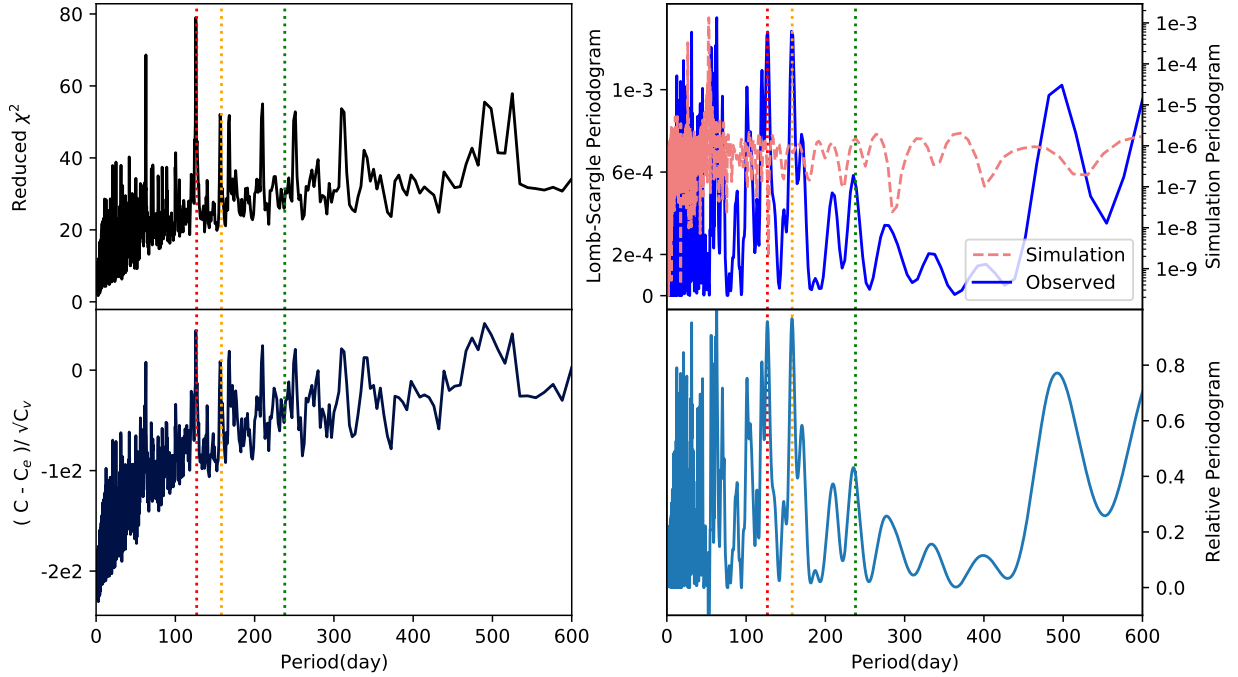


Figure 4. The period of SGR J1935+2154 derived from sample A. The left two panels show the result of reduced χ^2 and $(C - C_e)/\sqrt{C_v}$ of period folding. The Lomb-Scargle periodogram of observed bursts data and simulated data of observation windows shows in the right upper panel with blue line and lightcoral dashed line, respectively. We normalize these two periodogram with maximum power value, and subtract the normalized periodogram of simulated data from the observed one. The result is shown in the right lower panel. The vertical red dotted line indicate the peak of relative periodogram which is 126.88 day, which is also significant in the period folding results with the reduced χ^2 and $(C - C_e)/\sqrt{C_v}$ method. The vertical orange dotted and the vertical green dotted line represent 158.15 day and 238 day, respectively.

3.2 Lomb-Scargle Periodogram

The Lomb-Scargle Periodogram has been widely used in unevenly sampled data for searching periodicity (Lomb 1976; Scargle 1982; VanderPlas 2018). In this paper, we use the Lomb-Scargle function to search possible periodic window with test period spanning from 0.5 day to 600 day. The event rates mean that the burst numbers divided by exposure time and are calculated with a bin size of 0.05 day for stable False Alarm Probability (FAP) (see Zou et al. 2021). The results are shown with blue line in right upper panel of Fig 4 and 5, respectively. The most significant peak of the Lomb-Scargle periodogram is 127.30 day and 126.89 day for Sample A and B, respectively. We note that there are additional two non-negligible significant peaks around 157.2 day and 498.33 day. The FAP of each possible period are followings: $\text{FAP}(127.30 \text{ day}) = 3.39 \times 10^{-13}$, $\text{FAP}(157.2 \text{ day}) = 4.76 \times 10^{-13}$ and $\text{FAP}(498.33 \text{ day}) = 5.59 \times 10^{-10}$. However, these two peaks are much less significant in the results of Period Folding method (left panels of Fig 4 and 5). They are likely caused by observation windows and bursts gap, which will be discussed in Section 3.3.

We note that there is also a peak around 238 day, which is the favored period in previous studies (Denissenya et al. 2021; Grossan 2021; Zou et al. 2021), but the significance of this peak around 238 day is much lower than other peaks. This change of the significance of the period of 238 day is mostly caused by the inclusion of new bursts after 2021 October.

In addition, to test the effect of the observation window (see Fig. 2), we simulate a series of bursts in visible observation windows

of Fermi/GBM from 2014 July to 2022 January and calculate the Lomb-Scargle periodogram of these simulated bursts. The light coral dashed line represents the simulated data of observation windows in the right upper panel of Fig 4 and 5. There are two apparent peaks at 26.46 day and 52.95 day, which indicate that the periods around 26 day or 52 day are probably caused by the observation window effects.

We normalize the periodogram of observation bursts data and the periodogram of simulated bursts considering observation window effect with maximum power value (namely the power of Lomb-Scargle periodogram), and subtract the latter from the former. Then we get the relative periodogram (Zhang et al. 2021) which are shown in the right lower panels of Fig 4 and 5. The results of the relative periodogram of two samples are similar to the original periodogram. The prominent peaks of the relative periodogram of sample A are 55, 126.88 and 158 day, which are consistent with that of sample B.

According to the above results, we conclude that the most favored period is about 126.88 ± 2.05 day for Sample A and 127.02 ± 1 day for Sample B. The error is calculated with the same method in CHIME/FRB Collaboration et al. (2020a): $\sigma = PW_{\text{active}}/T_{\text{span}}$, where P is period and W_{active} is active days. For sample A, we show the folded phase histogram in Fig 6. The filled plum histogram is the phase profile of sample A, based on which we define the phases between $\varphi=0.05$ and $\varphi=0.4$ as the active window. Then, we plot the time history (in MJD) of Fermi/GBM and GECAM bursts, together with active windows for periods of 126.88 day (this work) and 238 day (reported in previous works, Denissenya et al. 2021; Grossan 2021; Zou et al. 2021), as shown in Fig 8. Most bursts fall in the

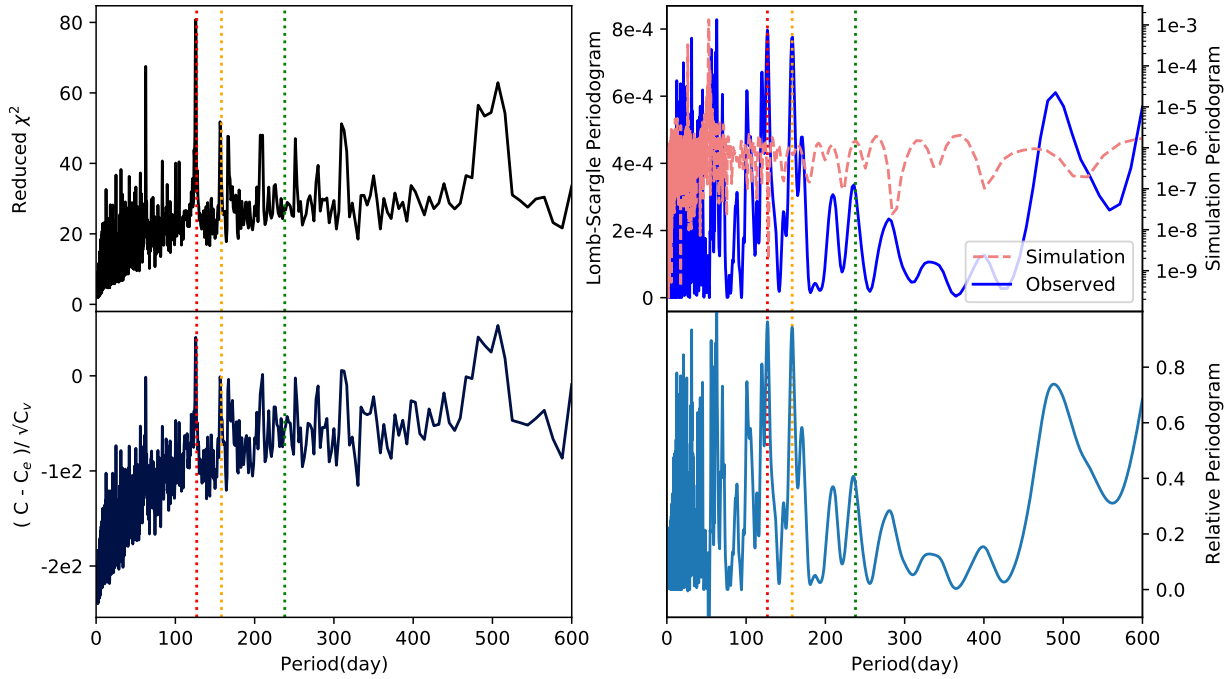


Figure 5. The period of SGR J1935+2154 derived from sample B. The left two panel show the result of reduced χ^2 and $(C - C_e)/\sqrt{C_v}$ of period folding. The Lomb-Scargle periodogram of observed bursts data and simulated data of observation windows shows in the right upper panel with blue line and lightcoral dashed line, respectively. We normalize these two periodogram with maximum power value, and subtract normalized periodogram of simulated data from observed one. The result show in the right lower panel. The vertical red dotted line indicate the peak of relative periodogram which is 127.02 day. It is consistent with the peak of reduced χ^2 and $(C - C_e)/\sqrt{C_v}$. The vertical orange dotted and the vertical green dotted line represent 158.15 day and 238 day, respectively

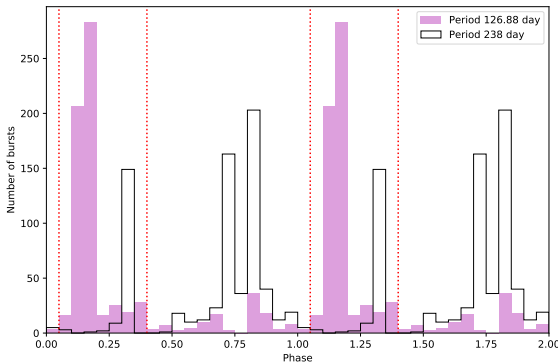


Figure 6. The folded phase of SGR J1935+2154. The plum histogram is the distribution of sample A with period 126.88 day. The active window (i.e. from $\varphi=0.05$ to $\varphi=0.4$) is denoted with red dotted lines. The black histogram represent the folding profile of Sample A with a period of 238 day (reported in previous studies [Denissenya et al. 2021](#); [Grossan 2021](#); [Zou et al. 2021](#)), which is disfavored by the present results.

active windows (see Fig 6), but some are outside, which are also shown in Fig 8. This may hint that the period behavior is not very strict, e.g. including some quasi-periodic behavior.

3.3 Simulation Tests

In this study, we test whether we can recover the input period in the burst series with the period folding and Lomb-Scargle periodogram methods used in this work. Especially we made two kinds of simulation tests to evaluate the effects of observation window and burst rate variation.

First, we set the input period as $P_{\text{simu}}=126.88$ day and then draw bursts according to the phase profile (see Fig 6) folded with this period of 126.88 day. Since we need to simulate bursts from 2014-01-01 to 2022-01-18, this time-span (8 years) contains about ~ 23 periods. In each period, we make sure that the simulated burst rate follow the profile of folded phase.

Then, we did three different classes of simulations, with 10 simulations for each class. As an example, one of the 10 simulations with the input period of 126.88 day is shown in Fig 7). For class 1, the total number of simulated bursts in each period is random (upper panel in Fig 7). For class 2, the total number of bursts is equal to the detected bursts of SGR J1935+2154 (middle panel in Fig 7). For class 3, removing those bursts in the invisible time windows from the class 2. Then we apply the same period analysis with the Period Folding and Lomb-Scargle periodogram methods to the simulated bursts data.

We find that these 10 simulations give similar results for both Lomb-Scargle periodogram and period folding methods, thus we calculate the average Lomb-Scargle periodogram, χ^2 -stat and C -stat test of these 10 simulations. The results of all three classes of simulation are shown in Fig 9. It shows that these periodicity search methods can successfully recover the input period (i.e. 126.88 day

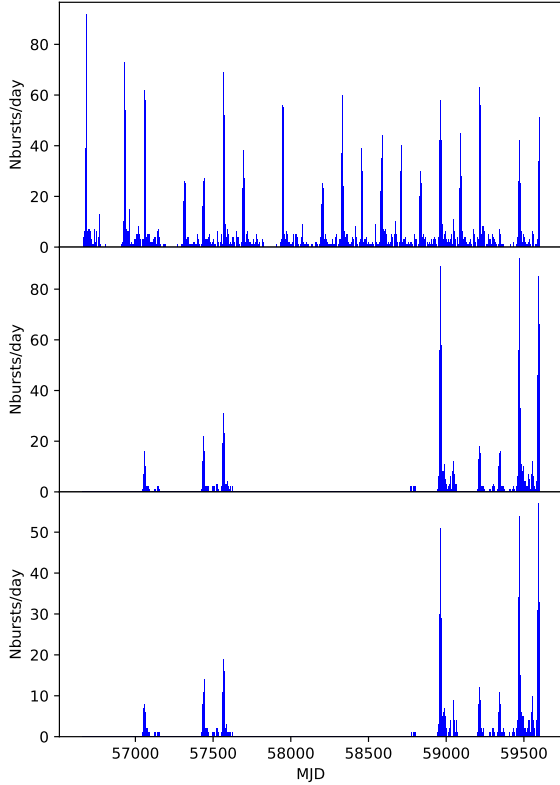


Figure 7. One of the 10 simulated burst data with an input period of 126.88 day as an example. The upper, middle and lower panel is the event rate of simulated bursts of Class 1, 2 and 3, respectively.

in this simulation). It also, as expected, shows several harmonic peaks of the input period. Interestingly, for class 2 and 3, both the periodogram and period folding show remarkable peaks around 498 day, while there are also lower significant peaks around the period of 158.15 day and 238 day. Since all these periods (i.e. 158.15, 238, and 498 day) are absent in the class 1, it seems that they are introduced by the burst rate variation or other observation effects.

Lastly, we repeat the above simulations with input period $P_{\text{simu}}=50, 100, 150, 200$ and 250 day, respectively. We find that the input period can be recovered by the periodicity search methods used in this study, which demonstrates that these methods of periodic analysis are reasonably reliable. Moreover, the Lomb-Scargle periodogram of some simulation periods (such as 50 day, 100 day, 150 day and 250 day) still show weak peaks around 125 day, 158 day, 238 day and 500 day. This indicates that the 126.88 day periodicity may be affected by observation factors as well.

4 DISCUSSIONS AND SUMMARY

The period behavior of repeating FRBs is still a mystery. Motivated by the connection between FRBs and SGRs, we analyze the possible active periodic window of bursts from SGR J1935+2154. In this paper, we adopt two methods to search the possible periodic window (Period Folding and Lomb-Scargle Periodogram) on the updated burst sample.

To acquire more samples for searching and constraining the active periodic window, we developed a targeted search pipeline to search Fermi/GBM data from 2008 August to 2014 December. Then we exclude the solar flares, particle events, TGFs and some spurious triggers (such as phosphorescence spike events), and find 10 candidate bursts. Although these candidate bursts are found with Fermi/GBM data only and lack of confirmed observation by other instruments, their properties (light curve, spectrum and locations) are well consistent with known bursts from SGR J1935+2154, suggesting that most of them should be likely from SGR J1935+2154. They are rather weak that Fermi/GBM could not trigger them. None of them were in the field of view of Swift/BAT, thus there is no expected detection by Swift/BAT as well.

We defined two burst samples: sample A contains high confidence bursts reported by Fermi/GBM and GECAM (from 2014 July to 2022 January), while sample B is composed of sample A and these 10 candidate bursts found from Fermi/GBM data between the year of 2018 and 2014. We mainly use sample A to do the periodicity search and sample for the cross check the result of sample A.

Based on the period analysis of observation data and simulations, we find the most favored period is 126.88 ± 2.05 day. The folded phase profile is shown in Fig 6, where the plum histogram is the phase for sample A, and the active window between $\varphi=0.05$ and $\varphi=0.4$ is given by Bayesian Block method. The burst history and phase are over-plotted in Fig 8 with the orange region representing the active window. It seems most of bursts lie in the active window including candidate bursts. There exist several peaks in the results of the searching periodic window. We implemented simulations to testify how the observation effects may interfere the period analysis. Our simulations suggest that the period around 55 day is a fake signal which is likely caused by observation windows, and the periods around 158, 238 and 498 day could be reproduced if considering the burst rate variation among periods.

Our results are very different from the periodicity ~ 238 day of previous studies (Grossan 2021; Denissenya et al. 2021; Zou et al. 2021), which is mostly because different studies used different burst samples. In this study, we added about 200 new bursts found in a few months Fermi/GBM data and almost one year GECAM data. We also tried to extend the burst history before the first previously reported burst by Swift/BAT in 2014, by targeted search Fermi/GBM data from 2008 to 2014. Another difference is that we studied the observation effects on the periodicity search by detailed simulations and found that these effects may introduce fake periods.

However, we should note that, as shown in Fig. 8, the periodicity 126.88 day is imperfect since the burst history of SGR J1935+2154 is very complicated and the burst rate varies drastically from time to time, even including some time epoch with none detection of any burst. This may hint that even though there is a period in the burst activity, the burst rate for some period epoch may be very low thus hardly to be observed. In any rate, it seems any robust conclusion regarding the periodicity of the burst behavior should heavily rely on more observations in the future.

One of the popular explanations for the PWB is that the repeating FRBs come from a magnetar in binary with a companion star (Ioka & Zhang 2020; Lyutikov et al. 2020; Zhang 2020a; Wang et al. 2022). The orbital motion of the binary leads to the periodic variation of the optical depth for the radio emission and, therefore, the radio emission can be observed only in a window during which the pulsar wind cavity is on the line of sight (Chen et al. 2021). However, there is actually no evidence supporting the existence of a companion star for SGR J1935+2154. Therefore, in principle, PWB may not be expected in the X-ray burst activity of SGR J1935+2154 if the PWB

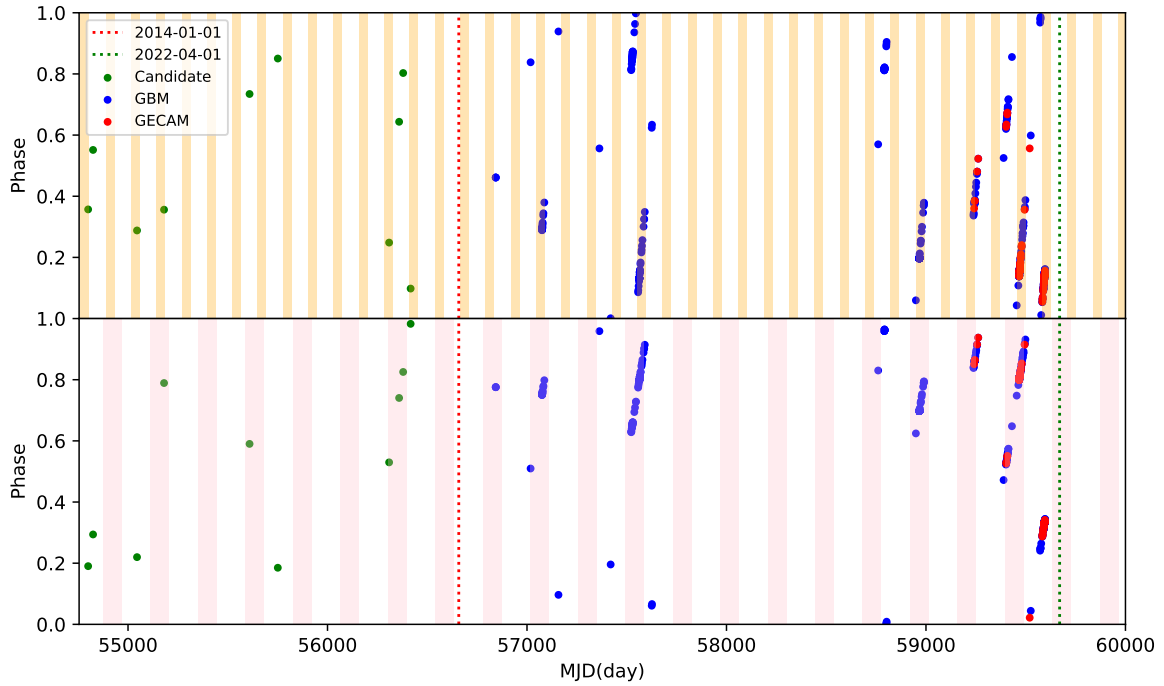


Figure 8. Upper panel: The burst times (MJD) and phase of SGR J1935+2154 with a period of 126.88 day. The orange shadow represent the active window in each period as shown in 6. The blue, red and green dots indicate the reported bursts of Fermi/GBM, GECAM and the targeted search candidate bursts of Fermi/GBM, respectively. Lower panel: The same with the upper panel but the period is set to 238 day and the pink shadow regions denote the active window (Zou et al. 2021).

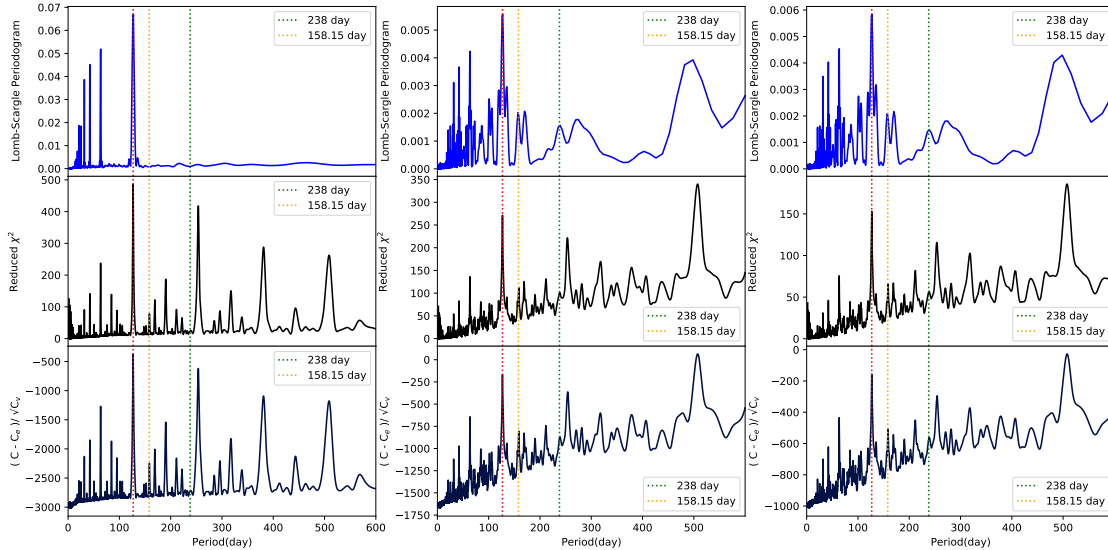


Figure 9. Period search on simulated bursts. The left, middle and right three panels are results for simulated burst data of Class 1, 2 and 3, respectively. The Lomb-Scargle periodogram and period folding with Pearson's χ^2 -stat test and C -stat test results are shown from top to bottom row panels. The red dotted line represent 126.88 day, i.e. the input period for the simulation. The orange and green dotted lines represent 158.15 day and 238 day, which are the apparent periods of Lomb-Scargle periodogram of sample A.

is primarily caused by the binary orbital motion. On the contrary, if the PWB indeed exists in SGR J1935+2154, then the PWB of the repeating FRBs might be also due to some other mechanisms (e.g., the precession of the magnetar; Levin et al. 2020; Zanazzi & Lai 2020; Chen 2020; Wasserman et al. 2022) rather than the binary orbital motion.

If the period of 126.88 day is real, considering that SGR J1935+2154 is unlikely to be in a binary system, then we argue that one possible reason for this period behavior could be the free precession of neutron star (Zanazzi & Lai 2020; Levin et al. 2020). The period of the free precession may be caused by a strong internal magnetic field or deviation of the rotation axis of the magnetar. The precession period of a magnetar is given by Levin et al. (2020),

$$P_{\text{pr}} \approx \frac{P_{\text{spin}}}{\epsilon} \approx 20 \left(\frac{k}{0.01} \right)^{-1} \left(\frac{B_{\text{int}}}{10^{16} \text{G}} \right)^{-2} \left(\frac{B_{\text{dip}}}{10^{15} \text{G}} \right) \left(\frac{t}{30 \text{yr}} \right)^{1/2} \text{ days} \quad (2)$$

where P_{prec} is the period of the free precession, P_{spin} is the spin period of the magnetar, k is the numerical coefficient, B_{int} is the internal magnetic field of the magnetar, B_{dip} is the surface dipole magnetic field, and t is the age of the magnetar. The maximum $k \approx 1$ would be approached if the field is fully coherent and purely toroidal. The value of k is reduced when the field is tangled. According to this equation, using our result $p_{\text{pr}} = 126.88$ day and $p_{\text{spin}} = 3.24$ s, $B_{\text{dip}} = 2.2 \times 10^{14}$ G, $t = 3.6$ kyr (Israel et al. 2016), we can derive that $\epsilon \approx 2.96 \times 10^{-7}$. If $k = 0.001$, the internal magnetic field is about 1.95×10^{15} G. In addition, the cause for period could be the force precession as discussed by some studies (Sob'yanin 2020; Tong et al. 2020; Yang & Zou 2020), e.g. the anomalous torque of electromagnetic forces induced by magnetar rotation could cause the precession; the torque caused by fallback disk (Tong et al. 2020) can enhance the precession and lead to a long period.

ACKNOWLEDGEMENTS

This work is supported by the National Key R&D Program of China (2021YFA0718500), the Strategic Priority Research Program on Space Science (Grant No. XDA15360102, XDA15360300, XDA15052700) of the Chinese Academy of Sciences, the National SKA program of China (2020SKA0120300), and the National Natural Science Foundation of China (Grant No. 11833003, 12173038).

DATA AVAILABILITY

The Fermi/GBM data used in this paper are available at <https://heasarc.gsfc.nasa.gov/FTP/fermi/data>. The GECAM data will be released at <http://gecam.ihep.ac.cn/>. All data and codes underlying this article will be shared on reasonable request.

Software: Python⁶; numpy⁷; matplotlib⁸; pandas⁹; scipy¹⁰; as-

trophy¹¹; Bayesian Blocks¹²; LombScargle¹³; GBM Data Tools¹⁴; GBM Response Generator¹⁵; Xspec¹⁶;

REFERENCES

- Banas K. R., Hughes J. P., Bronfman L., Nyman L. Å., 1997, *ApJ*, **480**, 607
 Bannister K. W., et al., 2019, *Science*, **365**, 565
 Blackburn L., Briggs M. S., Camp J., Christensen N., Connaughton V., Jenke P., Remillard R. A., Veitch J., 2015, *ApJS*, **217**, 8
 Bochenek C. D., Ravi V., Belov K. V., Hallinan G., Kocz J., Kulkarni S. R., McKenna D. L., 2020, *Nature*, **587**, 59
 Briggs M. S., et al., 2013, *Journal of Geophysical Research (Space Physics)*, **118**, 3805
 CHIME/FRB Collaboration et al., 2020a, *Nature*, **582**, 351
 CHIME/FRB Collaboration et al., 2020b, *Nature*, **587**, 54
 Cai C., et al., 2021, *MNRAS*, **508**, 3910
 Cao X.-F., Yu Y.-W., Dai Z.-G., 2017, *ApJ*, **839**, L20
 Chatterjee S., et al., 2017, *Nature*, **541**, 58
 Chen W.-C., 2020, *PASJ*, **72**, L8
 Chen A. M., Guo Y. D., Yu Y. W., Takata J., 2021, *A&A*, **652**, A39
 Connor L., Sievers J., Pen U.-L., 2016, *MNRAS*, **458**, L19
 Cordes J. M., Wasserman I., 2016, *MNRAS*, **457**, 232
 Cruces M., et al., 2021, *MNRAS*, **500**, 448
 Denissenya M., Grossan B., Linder E. V., 2021, *Phys. Rev. D*, **104**, 023007
 Duncan R. C., Thompson C., 1992, *ApJ*, **392**, L9
 Goldstein A., et al., 2019, arXiv e-prints, p. arXiv:1903.12597
 Grossan B., 2021, *PASP*, **133**, 074202
 Ioka K., Zhang B., 2020, *ApJ*, **893**, L26
 Israel G. L., et al., 2016, *MNRAS*, **457**, 3448
 Kaastra J. S., 2017, *A&A*, **605**, A51
 Kaspi V. M., Beloborodov A. M., 2017, *ARA&A*, **55**, 261
 Katz J. I., 2016, *ApJ*, **826**, 226
 Kouveliotou C., et al., 1998, *Nature*, **393**, 235
 Kulkarni S. R., Ofek E. O., Neill J. D., Zheng Z., Juric M., 2014, *ApJ*, **797**, 70
 Levin Y., Beloborodov A. M., Bransgrove A., 2020, *ApJ*, **895**, L30
 Li X., et al., 2021a, *Radiation Detection Technology and Methods*
 Li C. K., et al., 2021b, *Nature Astronomy*, **5**, 378
 Lin L., et al., 2020a, *Nature*, **587**, 63
 Lin L., Göğüş E., Roberts O. J., Kouveliotou C., Kaneko Y., van der Horst A. J., Younes G., 2020b, *ApJ*, **893**, 156
 Lin L., Göğüş E., Roberts O. J., Baring M. G., Kouveliotou C., Kaneko Y., van der Horst A. J., Younes G., 2020c, *ApJ*, **902**, L43
 Lomb N. R., 1976, *Ap&SS*, **39**, 447
 Lorimer D. R., Bailes M., McLaughlin M. A., Narkevic D. J., Crawford F., 2007, *Science*, **318**, 777
 Lu W., Kumar P., Zhang B., 2020, *MNRAS*, **498**, 1397
 Lyutikov M., 2017, *ApJ*, **838**, L13
 Lyutikov M., Barkov M. V., Giannios D., 2020, *ApJ*, **893**, L39
 Macquart J. P., et al., 2020, *Nature*, **581**, 391
 Marcote B., et al., 2017, *ApJ*, **834**, L8
 Marcote B., et al., 2020, *Nature*, **577**, 190
 Margalit B., Beniamini P., Sridhar N., Metzger B. D., 2020, *ApJ*, **899**, L27
 Meegan C., et al., 2009, *ApJ*, **702**, 791
 Mereghetti S., et al., 2020, *ApJ*, **898**, L29

¹¹ <https://www.astropy.org/>

¹² https://docs.astropy.org/en/stable/api/astropy.stats.bayesian_blocks.html

¹³ <https://docs.astropy.org/en/stable/timeseries/lombscargle.html>

¹⁴ https://fermi.gsfc.nasa.gov/ssc/data/analysis/rmfit/gbm_data_tools/gdt-docs/

¹⁵ <https://fermi.gsfc.nasa.gov/ssc/data/analysis/gbm/INSTALL.html>

¹⁶ <https://heasarc.gsfc.nasa.gov/xanadu/xspec/>

⁶ <https://www.python.org/>

⁷ <https://numpy.org/>

⁸ <https://matplotlib.org/>

⁹ <https://pandas.pydata.org/>

¹⁰ <https://scipy.org/>

Table 3. The SGR J1935+2154 burst sample detected by Fermi/GBM from 2021 November to 2022 January.

Burst Time (UTC)	Burst Time (UTC)	Burst Time (UTC)	Burst Time (UTC)	Burst Time (UTC)
2021-11-07T07:54:51.187	2021-12-24T03:42:34.341	2021-12-25T09:32:50.504	2021-12-25T18:48:28.387	2021-12-25T22:22:20.115
2021-12-26T12:55:09.689	2021-12-29T16:41:26.191	2022-01-04T00:42:17.704	2022-01-04T04:32:11.147	2022-01-05T06:01:31.350
2022-01-05T07:06:40.725	2022-01-06T02:36:14.044	2022-01-08T14:41:46.862	2022-01-09T04:57:16.080	2022-01-09T07:39:10.637
2022-01-09T09:28:12.737	2022-01-09T09:40:33.491	2022-01-09T09:55:20.779	2022-01-09T12:57:21.913	2022-01-09T14:16:08.559
2022-01-09T23:25:43.291	2022-01-10T02:57:16.776	2022-01-10T04:31:43.117	2022-01-10T15:55:38.291	2022-01-11T05:42:12.251
2022-01-11T07:48:21.419	2022-01-11T08:58:35.308	2022-01-11T17:05:55.630	2022-01-11T18:21:07.672	2022-01-11T21:54:01.124
2022-01-11T21:55:11.116	2022-01-12T01:03:46.329	2022-01-12T01:08:01.574	2022-01-12T02:05:58.212	2022-01-12T02:19:22.106
2022-01-12T04:10:05.302	2022-01-12T04:31:19.934	2022-01-12T05:42:51.470	2022-01-12T08:39:25.279	2022-01-12T08:48:28.544
2022-01-12T17:57:07.731	2022-01-12T18:12:04.642	2022-01-12T19:58:04.027	2022-01-12T23:00:12.748	2022-01-13T02:30:24.267
2022-01-13T02:37:06.879	2022-01-13T05:59:14.025	2022-01-13T06:49:04.357	2022-01-13T08:34:20.010	2022-01-13T08:37:42.154
2022-01-13T09:05:22.677	2022-01-13T10:28:58.992	2022-01-13T10:41:55.477	2022-01-13T13:07:30.634	2022-01-13T13:16:45.157
2022-01-13T14:35:34.417	2022-01-13T14:40:54.853	2022-01-13T14:44:57.928	2022-01-13T14:58:01.149	2022-01-13T15:13:25.807
2022-01-13T16:26:37.528	2022-01-13T19:23:10.210	2022-01-13T19:36:08.511	2022-01-13T19:57:55.715	2022-01-14T00:38:18.604
2022-01-14T04:02:38.208	2022-01-14T06:37:56.739	2022-01-14T08:16:01.323	2022-01-14T11:26:42.754	2022-01-14T11:39:41.804
2022-01-14T13:23:05.792	2022-01-14T13:34:30.163	2022-01-14T16:08:43.298	2022-01-14T19:27:16.671	2022-01-14T19:42:08.833
2022-01-14T19:45:08.047	2022-01-14T20:41:14.905	2022-01-14T20:46:16.444	2022-01-14T20:46:17.510	2022-01-14T20:46:32.943
2022-01-14T20:56:27.522	2022-01-14T22:21:29.360	2022-01-14T22:21:33.331	2022-01-14T22:38:26.261	2022-01-14T22:46:54.966
2022-01-15T00:03:17.918	2022-01-15T00:36:54.124	2022-01-15T03:08:22.219	2022-01-15T06:37:08.499	2022-01-15T06:44:05.437
2022-01-15T07:05:44.753	2022-01-15T07:08:43.476	2022-01-15T07:54:13.911	2022-01-15T07:54:43.936	2022-01-15T08:00:58.090
2022-01-15T08:04:45.318	2022-01-15T08:16:31.251	2022-01-15T08:21:46.394	2022-01-15T08:23:02.089	2022-01-15T08:24:36.044
2022-01-15T08:25:56.217	2022-01-15T08:27:38.893	2022-01-15T08:36:42.075	2022-01-15T08:36:51.475	2022-01-15T08:39:22.360
2022-01-15T08:45:40.673	2022-01-15T09:24:40.334	2022-01-15T09:26:39.856	2022-01-15T09:39:04.523	2022-01-15T09:43:00.887
2022-01-15T10:10:40.694	2022-01-15T12:50:12.834	2022-01-15T13:09:50.129	2022-01-15T13:13:05.353	2022-01-15T13:13:07.566
2022-01-15T16:06:05.370	2022-01-15T16:10:49.654	2022-01-15T17:21:59.283	2022-01-15T19:11:28.185	2022-01-15T19:19:46.057
2022-01-15T19:25:22.434	2022-01-15T19:27:50.194	2022-01-15T20:35:30.342	2022-01-15T22:38:44.484	2022-01-15T22:51:22.059
2022-01-16T03:14:35.947	2022-01-16T07:43:05.577	2022-01-16T10:03:57.580	2022-01-16T10:48:37.617	2022-01-16T10:59:28.693
2022-01-16T11:15:52.747	2022-01-16T11:17:35.433	2022-01-16T11:20:30.636	2022-01-16T11:30:23.385	2022-01-16T11:39:42.753
2022-01-16T12:23:46.018	2022-01-16T12:38:23.736	2022-01-16T14:09:38.568	2022-01-16T14:10:01.110	2022-01-16T18:46:30.292
2022-01-17T01:27:12.687	2022-01-17T01:39:37.260	2022-01-17T12:43:01.185	2022-01-17T15:37:58.722	2022-01-17T18:39:49.468

Table 4. The SGR J1935+2154 burst sample detected by GECAM from 2021 January to 2022 January.

Burst Time (UTC)	Burst Time (UTC)	Burst Time (UTC)	Burst Time (UTC)	Burst Time (UTC)
2021-01-27T06:50:20.750	2021-01-30T08:39:53.840	2021-01-30T10:35:35.120	2021-02-11T13:43:16.760	2021-02-16T22:20:39.600
2021-07-07T00:33:31.640	2021-07-08T00:18:18.560	2021-07-12T04:32:39.600	2021-07-12T22:12:58.100	2021-09-09T21:07:12.150
2021-09-10T01:04:33.500	2021-09-10T02:07:56.700	2021-09-10T02:08:28.800	2021-09-10T03:22:40.550	2021-09-10T03:24:47.150
2021-09-10T03:42:45.750	2021-09-10T05:05:03.350	2021-09-10T05:35:55.500	2021-09-11T16:35:46.500	2021-09-11T16:39:21.000
2021-09-11T16:50:03.850	2021-09-11T17:01:10.800	2021-09-11T17:01:59.550	2021-09-11T17:04:29.800	2021-09-11T17:10:48.750
2021-09-11T18:02:13.500	2021-09-11T18:04:46.350	2021-09-11T18:54:36.050	2021-09-11T19:43:28.000	2021-09-11T19:46:50.050
2021-09-11T20:13:40.550	2021-09-11T20:22:59.050	2021-09-11T20:33:14.550	2021-09-11T21:07:28.350	2021-09-11T22:51:41.600
2021-09-12T00:34:37.450	2021-09-12T00:45:49.400	2021-09-12T05:14:07.950	2021-09-12T05:44:17.050	2021-09-12T16:26:08.150
2021-09-12T16:52:07.950	2021-09-12T22:16:36.200	2021-09-13T00:27:25.200	2021-09-13T14:12:39.650	2021-09-13T19:51:33.350
2021-09-14T11:10:36.250	2021-09-14T14:15:42.900	2021-09-14T23:21:58.500	2021-09-14T23:26:34.050	2021-09-15T02:39:25.700
2021-09-15T15:32:56.050	2021-09-17T12:52:37.800	2021-09-17T13:58:25.100	2021-09-18T22:58:52.150	2021-09-22T02:39:10.200
2021-09-22T20:12:16.500	2021-10-07T11:57:07.700	2021-11-01T23:13:41.950	2022-01-04T04:32:11.200	2022-01-05T06:01:31.450
2022-01-05T07:06:40.800	2022-01-06T02:36:14.100	2022-01-08T14:41:46.900	2022-01-09T07:39:10.700	2022-01-10T06:52:40.500
2022-01-11T08:58:35.450	2022-01-12T01:03:46.900	2022-01-12T05:42:51.650	2022-01-12T08:39:25.450	2022-01-12T17:57:08.500
2022-01-13T19:36:08.600	2022-01-13T20:14:58.600	2022-01-13T21:41:17.900	2022-01-14T19:42:08.833	2022-01-14T19:45:08.100
2022-01-14T19:56:52.700	2022-01-14T20:06:07.400	2022-01-14T20:07:03.050	2022-01-14T20:12:45.300	2022-01-14T20:15:54.400
2022-01-14T20:21:05.150	2022-01-14T20:23:35.400	2022-01-14T20:26:50.300	2022-01-14T20:29:07.250	2022-01-14T20:31:49.900
2022-01-15T09:26:39.900	2022-01-15T13:52:26.050	2022-01-15T16:31:14.900	2022-01-15T17:21:59.300	2022-01-16T10:48:37.650
2022-01-17T01:39:37.300	2022-01-23T20:06:38.750	2022-01-24T02:10:55.050	2022-01-24T02:27:07.400	

Metzger B. D., Berger E., Margalit B., 2017, *ApJ*, **841**, 14Michilli D., et al., 2018, *Nature*, **553**, 182Petroff E., et al., 2016, *Publ. Astron. Soc. Australia*, **33**, e045Platts E., Weltman A., Walters A., Tendulkar S. P., Gordin J. E. B., Kandhai S., 2019, *Phys. Rep.*, **821**, 1Popov S. B., Postnov K. A., 2010, in Harutyunian H. A., Mickaelian A. M., Terzian Y., eds, *Evolution of Cosmic Objects through their Physical*Activity, pp 129–132 ([arXiv:0710.2006](https://arxiv.org/abs/0710.2006))Rajwade K. M., et al., 2020, *MNRAS*, **495**, 3551Ravi V., et al., 2019, *Nature*, **572**, 352Ridnaia A., et al., 2021, *Nature Astronomy*, **5**, 372Scargle J. D., 1982, *ApJ*, **263**, 835Sob'yanin D. N., 2020, *MNRAS*, **497**, 1001Spitler L. G., et al., 2016, *Nature*, **531**, 202

- Stamatikos M., Malesani D., Page K. L., Sakamoto T., 2014, GRB Coordinates Network, [16520, 1](#)
- Tavani M., et al., 2020, The Astronomer's Telegram, [13686, 1](#)
- Tendulkar S. P., et al., 2017, [ApJ, 834, L7](#)
- Thornton D., et al., 2013, [Science](#), 341, 53
- Tong H., Wang W., Wang H.-G., 2020, [Research in Astronomy and Astrophysics](#), 20, 142
- VanderPlas J. T., 2018, [ApJS, 236, 16](#)
- Wang F. Y., Zhang G. Q., Dai Z. G., Cheng K. S., 2022, arXiv e-prints, p. [arXiv:2204.08124](#)
- Wasserman I., Cordes J. M., Chatterjee S., Batra G., 2022, [ApJ, 928, 53](#)
- Wu Q., Zhang G. Q., Wang F. Y., Dai Z. G., 2020, [ApJ, 900, L26](#)
- Wu B., Zhang Y., Li X., Zhao H., Ge M., Liu C., Song L., Qu J., 2022, [Experimental Astronomy](#),
- Xiao S., et al., 2022, [MNRAS](#),
- Xiong S., et al., 2012, [Journal of Geophysical Research \(Space Physics\)](#), 117, [A02309](#)
- Yang H., Zou Y.-C., 2020, [ApJ, 893, L31](#)
- Yang Y.-P., Zhu J.-P., Zhang B., Wu X.-F., 2020, [ApJ, 901, L13](#)
- Yang Y.-H., et al., 2021, [ApJ, 906, L12](#)
- Younes G., et al., 2017, [ApJ, 847, 85](#)
- Younes G., et al., 2020, [ApJ, 904, L21](#)
- Yu Y.-W., Zou Y.-C., Dai Z.-G., Yu W.-F., 2021, [MNRAS, 500, 2704](#)
- Zanazzi J. J., Lai D., 2020, [ApJ, 892, L15](#)
- Zhang B., 2020a, [Nature](#), 582, 344
- Zhang B., 2020b, [Nature](#), 587, 45
- Zhang G. Q., Tu Z.-L., Wang F. Y., 2021, [ApJ, 909, 83](#)
- Zou J.-H., Zhang B.-B., Zhang G.-Q., Yang Y.-H., Shao L., Wang F.-Y., 2021, [ApJ, 923, L30](#)
- van Kerkwijk M. H., Kulkarni S. R., Matthews K., Neugebauer G., 1995, [ApJ, 444, L33](#)

This paper has been typeset from a $\text{\TeX}/\text{\LaTeX}$ file prepared by the author.